Applied Catalysis B: Environmental 304 (2022) 120961

Contents lists available at ScienceDirect

Applied Catalysis B: Environmental

journal homepage: www.elsevier.com/locate/apcatb

Catalytic activity of plasma-deposited Co_3O_4-based thin films for CO_2 hydration – A new approach to carbon capture applications

Hanna Kierzkowska-Pawlak, Ewelina Kruszczak, Jacek Tyczkowski *

Department of Molecular Engineering, Faculty of Process and Environmental Engineering, Lodz University of Technology, Wolczanska 213, 90-924 Lodz, Poland

ARTICLE INFO

Keywords:
Plasma deposition (PECVD)
Thin-film catalysts
Cobalt oxides
CO_2 hydration
Water clusters

ABSTRACT

Addressing the challenge of increasing the rate of CO_2 capture by accelerating the hydration process, we proposed the use of a new class of heterogeneous inorganic catalysts for this purpose. The presented research focused on Co_3O_4-based nanocatalysts produced by low-pressure plasma deposition (PECVD) in the form of thin films that can be deposited on any structured packing. The kinetic studies of this process were performed by bubbling CO_2 through pure water with catalytic or inert packing, measuring changes in pH value over time. The developed kinetic model described the experimental data very well and showed that the reaction at the interface between the CO_2 bubble and the catalyst surface is responsible for the catalytic effect. Studies of the molecular structure of the catalyst surface, carried out by the XPS technique, showed that the chemisorbed H_2O clusters on this surface are the active centers for the interaction with gaseous CO_2.

1. Introduction

We have long been accustomed, when discussing man-made carbon dioxide, to assign it a particularly negative role in global warming and the absolute necessity of its removal from the atmosphere [1]. However, on the other hand, we can look at CO_2 as a source of "pure" carbon – a wonderful substrate for the synthesis of various valuable products [2]. Let us take the example from plants that have been using carbon dioxide for at least two billion years instead of soil organic carbon to synthesize the needed organic compounds [3].

However, if we are going to utilize CO_2, we should first capture it from the atmosphere or industrial gases and concentrate to recover high-purity CO_2. Although many methods of CO_2 separation are being explored, its capture by reactive absorption using aqueous solutions of different amines is currently the most feasible approach [4]. Once the CO_2 encounters the liquid phase, it can enter into chemical reactions via various pathways depending on the amine type. In general, however, in many such cases, where water is used as a solvent, the hydration of CO_2, which we understand as the totality of phenomena, starting from the gas-liquid mass transfer through a set of CO_2 reactions and ending with the formation of the bicarbonate ion (HCO_3^-) as the main product, has been identified as the rate-determining step (bottleneck) in the CO_2 capture process [5,6]. No wonder, then, that much effort is being made to increase the rate of bicarbonate formation. It is quite clear that increasing the rate of CO_2 hydration would increase the overall rate of CO_2 binding in aqueous solutions, thereby improving the CO_2 capture performance. Besides, considering its subsequent sequestration through mineralization into environmentally friendly carbonates [7], the process of CO_2 hydration has also been identified as the most important step that needs to be accelerated.

The dissolution of gaseous CO_2 in water follows the pathways as shown in Fig. 1 [6–9]. The reaction *1* describes the process of $CO_{2(g)}$ transferring to $CO_{2(aq)}$, which is associated with the CO_2 mass transfer from the gas to the liquid phase. Subsequently, the CO_2 reacts in the liquid phase via two paths: path (I) with water molecules according to the consecutive chemical reactions (reactions *2–3*) leading to H^+ and HCO_3^- formation, or path (II) with hydroxide ions (reaction *4*) also forming bicarbonate ions. The carbonic acid H_2CO_3 formed directly in reaction *2* is very unstable and dissociates immediately into H^+ and HCO_3^- ions. The forward reaction rate constant of CO_2 with water (reaction *2*) is much lower than with hydroxide (reaction *4*) [8]. In fact, the relative contribution of paths (I) and (II) to the formation of HCO_3^- depends on pH. At values of pH lower than 8, due to the low concentration of hydroxide ions, the CO_2 hydration follows the water path according to reactions *2-3* and it is justified to neglect the second path of HCO_3^- formation via reaction *4* [4,8,10]. Moreover, due to the very low value of the dissociation constant of the bicarbonate, the reaction *5* is also often neglected. Thus, if CO_2 is dissolved in pure water, the

* Corresponding author.
E-mail address: jacek.tyczkowski@p.lodz.pl (J. Tyczkowski).

https://doi.org/10.1016/j.apcatb.2021.120961
Received 19 July 2021; Received in revised form 11 October 2021; Accepted 22 November 2021
Available online 25 November 2021

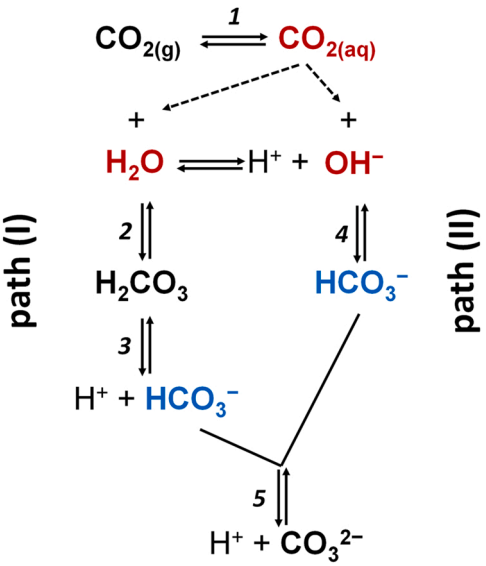

Fig. 1. The reaction scheme of CO_2 hydration.

formation of H^+ and HCO_3^- is favored through the water path (I).

In the past, a wide range of homogeneous catalysts, such as arsenate, arsenite, borate and vanadate inorganic oxoanions have been studied to enhance the hydration of CO_2 in aqueous solution [11–13]. In an attempt to overcome their drawbacks including problematic reusability due to their soluble form and toxicity, other approaches are also being investigated, for example biocatalysts immobilized on solid supports [14]. In particular, different variants of carbonic anhydrase enzymes have been intensively explored as effective catalysts for accelerating the CO_2 hydration. Carbonic anhydrase (CA) is the general name of water-soluble metalloproteins containing a Zn^{2+} ion as the active site, which facilitate the CO_2 transport in living organisms. The CA biocatalysts are receiving special attention due to the very high activity in catalyzing the conversion of CO_2 into bicarbonate via the water path (I) at turnover rates up to 10^6 s^{-1}. However, the reported rates are limited by the transfer of $CO_{2(g)}$ to $CO_{2(aq)}$ [14,15].

Despite significant advances in the use of enzymes for the capture and mineralization of CO_2, current research is still addressing their limitations, such as low stability under practical conditions, reduced activity after immobilization on a solid support and the problem of reuse [14–17]. Therefore, numerous attempts are being made to produce synthetic replications of the carbonic anhydrase active site. However, the catalytic activity of such organometallic bioanalogues in water phase reactions is significantly lower compared to the "real" carbonic anhydrase [6,18,19].

A new way to enhance the CO_2 hydration by nickel nanoparticles (NiNPs) has recently been reported by Bhaduri et al. [10,20]. However, the proposed concept is much less effective than the CA catalysts and requires an additional operation to separate the NiNPs from the CO_2 loaded solvent. Furthermore, the reported catalytic effect of NiNPs on the CO_2 hydration has been questioned [21,22]. Although the experiments demonstrated that NiNPs addition increased the CO_2 absorption flux in water, the observed enhancement could be possibly a consequence of the hydrodynamic effects in the resulting nanofluid than the catalytic activity of the added nanoparticles [23,24].

Taking on the challenge of enhancing CO_2 hydration through a solution that is also intended to offer potential practical application, the present studies have focused on the search for and development of suitable inorganic catalysts for this purpose. Catalytic materials produced by the non-equilibrium plasma technique (PECVD) deserve special attention in this respect [25,26]. Two particularly important features distinguish this technique from other methods of production of catalysts. Firstly, it enables the deposition of very thin catalytic films (below 1 μm) on virtually any substrate, which significantly broadens the horizons of their practical application, and secondly, the specificity of this method allows for a wide range of design at the molecular level and production of catalytic films with the desired composition and structure, which opens up unlimited possibilities to search for completely new, unique catalytic systems. To start with, cobalt oxides (CoO_X)-based thin films fabricated by the cold plasma deposition technique were proposed. These films have already proven themselves as catalysts in the CO_2 hydrogenation reactions [27,28]. Generally, cobalt oxides are also known as active materials in the process of water oxidation [29]. Bearing in mind the practical aspect, the films were deposited on wire-mesh supports. In industrial applications, such kind of metallic supports constitutes a starting substrate for constructing efficient structured packings in absorption columns used for CO_2 capture in aqueous solvents [4]. If such a packing is coated with a thin-film catalyst designed to enhance CO_2 hydration, it can improve the overall efficiency of CO_2 capture by aqueous solvents.

2. Experimental section

2.1. Catalyst preparation

The CoO_X-based thin films were produced by the plasma enhanced chemical vapor deposition (PECVD) in a parallel-plate radio-frequency (RF 13.56 MHz) reactor (schematically presented in Fig. 2a) from cobalt (I) cyclopentadienyldicarbonyl precursor ($CpCo(CO)_2$, Sigma-Aldrich, USA) (Fig. 2b(1)). This precursor is a source of cobalt, carbon, oxygen and hydrogen – the elements comprising the chemical structure of the deposited films. The plasma deposition was carried out in a mixture of the precursor and argon (99.999%, Linde Gas, Poland) with $CpCo(CO)_2$ and Ar flow rates of 0.083 and 0.71 sccm, respectively. The total pressure inside the reactor during the plasma process was approx. 4.0 Pa at the glow discharge power of 60 W. The support temperature reached about 320 K after one hour of the deposition process. The films for catalytic tests were deposited for 1 h on each site of circular gauze sheets (4 cm in diameter) made of kanthal wire used as supports (for details, see Section 2.2). For chemical structure investigations and wettability measurements, kanthal plates (1 × 1 cm^2) were used as a support, on which the catalytic films were deposited also for 1 h. Then, the as-deposited samples were heat treated in air or argon atmosphere at 773 K for 2 h to obtain active forms of cobalt oxides, according to our previous paper [27].

2.2. Support preparation

Knitted gauzes (mesh: 24 × 20 per inch) made of kanthal wire (0.11 mm in diameter, Kanthal AF – FeCrAl alloy (TermTech, Poland)) (Fig. 2c), as well as plates from the same kanthal alloy were used as the catalyst supports. Prior to the catalytic film deposition, the meshes and plates were subjected to heat treatment in air at 1173 K for 48 h. The aim of this process was to obtain a highly dispersed layer of alumina on the support to increase its surface area [30,31].

For comparative measurements, in which the CO_2 hydration process with an inert support without the catalyst film was tested, to ensure the catalytic passivity of its surface, as well as the same hydrodynamic conditions as in the case with the catalyst, the meshes (and the plates for wettability measurements) were subjected to appropriate plasma treatment. First, the supports were coated with a thin film deposited by plasma from allyl alcohol (AAL, ≥99%, Sigma-Aldrich, USA) as a precursor (Fig. 2b(2)), in the same reactor in which CoO_X-based films were prepared (Fig. 2a). The deposition was carried out without AAL vapor flow at its initial pressure of 3.5 Pa, with a discharge power of 10 W, for 180 s (on the meshes from both sides). Then, the produced films were treated with oxygen plasma, which allows to modify the surface wettability in a controlled manner and obtain hydrophilicity analogous to the surface of catalytic films. The treatment was performed using a

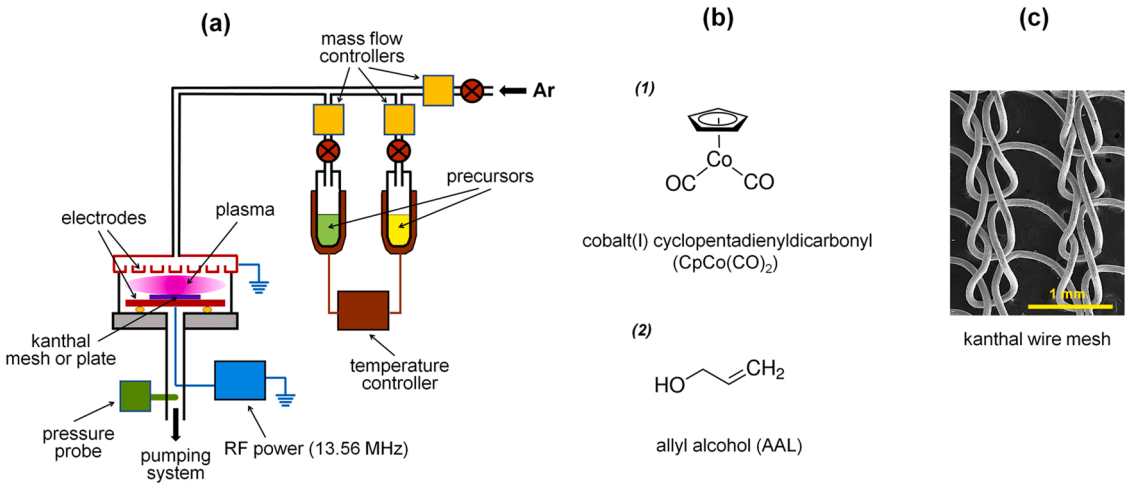

Fig. 2. (a) Schematic diagram of the RF plasma reactor for the deposition of thin films; (b) Chemical formulas of precursors; (c) Knitted kanthal gauze used as supports.

discharge power of 40 W and an O_2 flow rate of 4.0 sccm for 60–210 s. Details of the wettability measurements and their results are presented in Appendix (A.1).

2.3. CoO_X-based films stability tests in water

The structure of an effective catalyst for the CO_2 hydration requires a water-insoluble active phase. For measuring the stability of the CoO_X-based thin films when in contact with aqueous solutions, the individual samples were immersed in distilled and degassed water for 54 h at a constant temperature of 298 K. Using the electrode (ESAgP-341WhdM, Eurosensor-Poland), the pH of the solution was measured under the continuous bubbling of argon through the solution. Besides, the stability of the inert support, i.e. the mesh coated with AAL-polymer, was also tested. For the first hour of measurements, the pH value was recorded every 2 s, then every 10 min.

2.4. Catalyst testing

The catalytic activity of the CoO_X-based thin films (which reveal appropriate stability in water) was tested in the CO_2 hydration process carried out in distilled and degassed water. The process proceeds with a decrease in the pH of the solution due to the formation of H^+ ions, as shown in the reaction scheme in Fig. 1. Therefore, the rate of this process can be measured by the delta pH method, which has also been used in other studies focused on enhancing the CO_2 absorption in aqueous solutions [6,10,18,32,33].

The experiments were performed in a 200 mL glass reactor (shown in Fig. 3) filled with 150 mL of distilled water. The reactor was immersed in a thermostated water bath to maintain a constant reaction temperature of 298.0 ± 0.2 K. The gas was fed to the reactor through a G3 porosity sintered glass sparger (CTechGlass, USA) to obtain finely dispersed gas bubbles which improved mixing and increased the gas-liquid interfacial area. A circular sheet of the mesh (4 cm in diameter, with a geometrical active wire surface of 24.5 cm^2), either with or without the catalytic film (inert mesh), was attached 2.0 cm above the gas sparger. The pH electrode (the same as in the stability tests (Section 2.3)) mounted in an axial position, measured the pH of the liquid during the gas was bubbling through the water. The position of the mesh sheet and the electrode was always kept the same (with a distance of 1 cm between them).

Before starting the CO_2 hydration experiment, the water was purged with argon to remove residual amounts of dissolved gases until a stable pH value of about 6.65 was achieved. Then, the argon flow was stopped and dosing of CO_2 (99.998%, Linde Gaz, Poland) was started through a mass flow controller (model 5866, Brooks Instrument, USA) at a flow rate in the range of 50–170 mg/min under atmospheric pressure. The process was carried out until the physicochemical equilibrium was achieved, which was indicated by the stabilization of the pH value (at about pH = 3.93). For the same experimental conditions, five

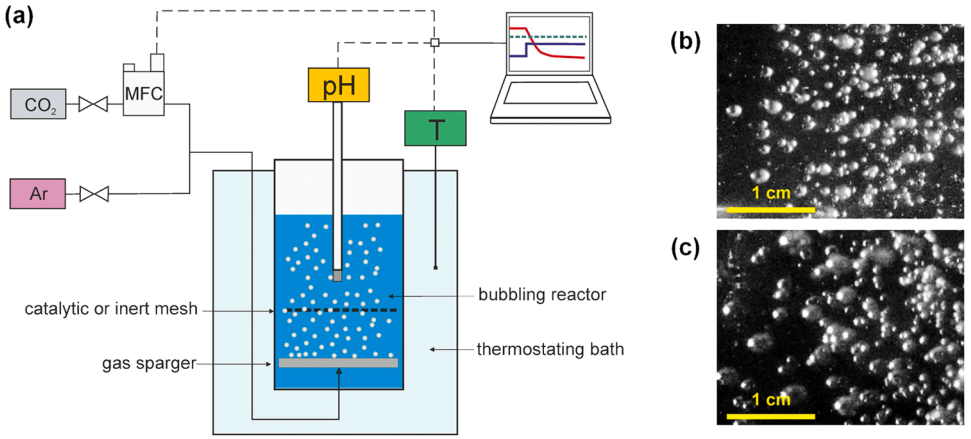

Fig. 3. (a) Schematic diagram of experimental set-up for CO_2 hydration studies (MFC – mass flow controller, pH – pH meter, T – temperature controller); (b) and (c) Typical bubble sizes for CO_2 flow rates of 54 mg/min and 170 mg/min, respectively.

consecutive measurement series were performed. The pH value was recorded every 2 s.

It should be emphasized that in the experiments, with both the catalyst-coated mesh and the inert mesh with the same shape and the same surface wettability, identical hydrodynamic conditions are maintained for a given CO_2 flow rate, such as gas hold-up, bubble size distribution and specific interfacial area. Therefore, the proposed methodology enables a clear and straightforward comparison between the kinetics of the CO_2 hydration with the thin film of catalyst and the inert mesh (without catalyst) in terms of the rate of H^+ formation while keeping the same hydrodynamics in both cases. By comparing two of the same mesh systems, one with the catalyst and the other without it (which serves as a reference), we can unequivocally demonstrate the activity of the catalyst. On the other hand, the use of a different reference system, for example the reactor without any mesh (CO_2 and water only) is unjustified, because the test would be carried out here not only without the catalyst, but also under completely different hydrodynamic conditions, which also determine the kinetics of the CO_2 hydration process. Thus, maintaining the same hydrodynamic conditions in systems with and without a catalyst is crucial in such tests.

2.5. Chemical structure analysis of the catalyst surface

The chemical structure of the surface of catalytic films was investigated by X-ray photoelectron spectroscopy (XPS), using an AXIS Ultra spectrometer (Kratos Analytical Ltd., UK) with monochromatic Al Kα X-rays (1486.6 eV). The spectra were collected from at least five different areas (300 × 700 μm^2) of each sample. The power of the anode was set at 180 W and the hemispherical electron energy analyzer was operated at a pass energy of 20 eV for all the high-resolution measurements. All the measurements were carried out using a charge neutralizer, and the main carbon peak (graphitic C 1 s at 284.6 eV) was taken for a final calibration of each spectrum.

The analysis of the chemical structure of the surface of catalytic films was performed for samples without and after contact with liquid water. The water-treated samples were immersed in distilled and degassed water at 298 K for a specified period of 2–54 h. The samples were then air dried at room temperature and the XPS measurements were carried out after 15 h. An analogous procedure as above was also used to determine the chemical structure of the catalyst surface after contact with liquid water and bubbled CO_2.

3. Results and discussion

3.1. Sample characterization

Our research, previously carried out using XPS and Raman spectroscopies, electron diffraction, and SEM and interference microscopies, allowed us to determine the details of chemical structure, nanostructure, and morphology of the deposited films, and above all showed that the heat treatment in air leads to the transformation of amorphous CoO_X contained in the as-deposited films into the Co_3O_4 form, while the treatment in argon to the form of CoO, embedding both these forms of cobalt oxides in a carbon matrix [27, and references therein].

Before carrying out experiments on the CO_2 hydration, we investigated the stability of CoO_X-based films after immersion in degassed water (see Section 2.3). The results obtained for samples with the Co_3O_4 (approx. 750 nm thick) and CoO (approx. 1500 nm thick) films are shown in Fig. 4. The pH value of the solution did not change with time after the mesh coated with the Co_3O_4-based film was immersed in water. It was stable at the level of 6.65 ± 0.02. In contrast, immersion of the mesh with CoO-based film in water with an initial pH of about 6.65 resulted in a gradual increase in pH, indicating the dissolution of CoO. Repeated testing on the same CoO sample re-immersed in pure water confirmed this adverse effect. The instability of the CoO-based film excludes it from research in processes involving an aqueous environment,

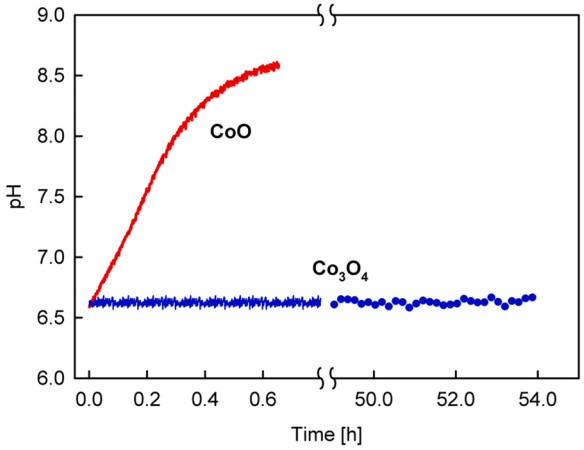

Fig. 4. Stability of CoO- and Co_3O_4-based films in pure water at 298 K.

while the mesh coated with a Co_3O_4-based film, identified as a stable solid phase, was further investigated in the CO_2 hydration process.

Another problem concerns the effect of the mesh nature on the passage of CO_2 bubbles through it. Be aware that different wettability of the mesh surface can affect the pattern of the bubbles passing through it, and thus the rate of CO_2 hydration [34,35]. As mentioned in Section 2.2, to exclude the influence of the mesh wettability on the CO_2 hydration rate, a reference mesh was prepared (without the Co_3O_4 film), which was covered with a plasma-deposited film from AAL (approx. 750 nm thick). The film was then treated with an oxygen plasma until the surface contact angle was the same as for the Co_3O_4 film, i.e. about 8°. The mesh produced in this way (inert mesh) did not show any changes in the pH of pure water (stable at 6.65 ± 0.02) in which it was immersed, while at the same time it was characterized by the same dynamics of CO_2 bubbles passing through it as in the case of the mesh with the Co_3O_4 film.

3.2. Kinetics of the CO_2 hydration process

Exemplary measurement results of CO_2 hydration efficiency as a function of time, starting from pH = 6.65 ± 0.02 for pure water, in the presence of both the mesh with the Co_3O_4-based film and the inert mesh, are shown in Fig. 5a. Despite slight differences, consistently lower pH values are evident for the Co_3O_4 case, until the both series of experiments, with and without the Co_3O_4 film, give the same value of pH = 3.93 ± 0.02, which indicates that finally the same equilibrium state has been reached (this calculated value is pH = 3.91 (Appendix (A.2)). To better visualize the differences in the hydration process with and without the Co_3O_4 film, the results from Fig. 5a were converted to the concentration of hydrogen ions (Fig. 5b).

The increase in H^+ concentration should be attributed to the formation of H^+ and, consequently, also HCO_3^- ions according to the path (I) of the CO_2 hydration (Fig. 1). The comparison of the course of this process in the presence of the catalytic film and its absence for the experiments carried out under the same hydrodynamic conditions at a given CO_2 flow rate (see Section 2.4) shows a difference in its rate. Taking both tracks into account in Fig. 5b, the change in H^+ concentration in the presence of the Co_3O_4 film is clearly faster than that without it. This is particularly noticeable for the range of 650 − 850 s, in which the track for the mesh with the catalyst (red curve) has a practically constant value of H^+ concentration, which indicates that this value was reached in less than 650 s. On the other hand, the track for the inert mesh (green curve) does not reach this value until around 800 s. There is no doubt that the observed enhancement of H^+ formation is due to the presence of the Co_3O_4 film, which should be credited with acting as a real catalyst in the hydration process. Indeed, the Co_3O_4-based film, like any catalyst, modifies the kinetics of the process by increasing its rate, but does not change its thermodynamic equilibrium.

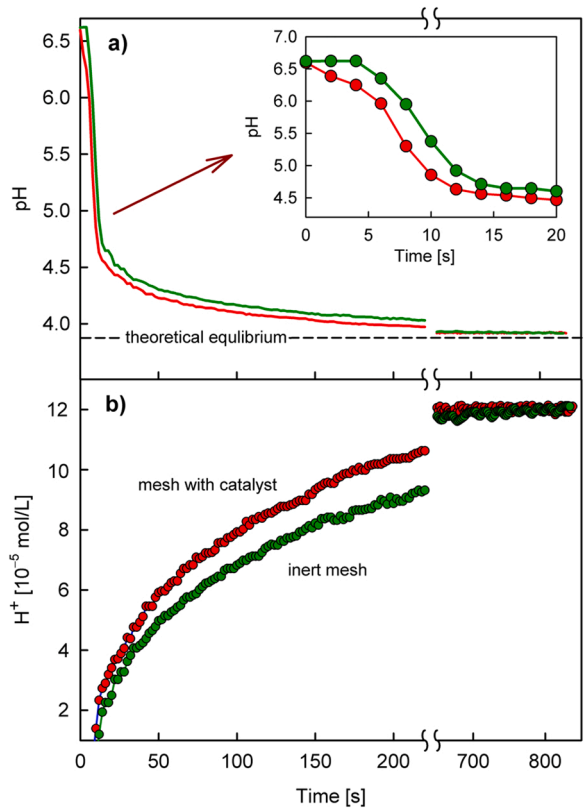

Fig. 5. Exemplary time course of CO_2 hydration in pure water (at CO_2 flow rate of 170 mg/min) in the presence of a mesh with the Co_3O_4-based film (red data) and inert mesh (green data). (a) pH measurements. Experimental equilibrium value very close to the calculated value (dashed line) is reached after approx. 800 s; (b) Data from figure (a) converted to the concentration of hydrogen ions. (For interpretation of the references to colour in this figure, the reader is referred to the web version of this article)

The rate of change in H^+ concentration provides a measure of the overall rate of the CO_2 hydration process. To quantify the observed catalytic acceleration of this process and to advance our understanding of its mechanism, we have developed a simplified mathematical model of the CO_2–water interaction under unsteady state conditions. In general, the model is based on the basic principles of mass balance for CO_2 absorption with reversible chemical reactions. Due to our experiments carried out in the range of pH<8, as already explained in Section 1, the model has been limited to path (I) (Fig. 1).

The first step in the CO_2 hydration process is the mass transfer from the gaseous CO_2 to another phase. We mean here both the typical absorption in the liquid water phase and, for example, adsorption on a hydrated solid surface, which, as it will turn out, takes place in our case with the catalyst. This mass transfer is expressed by the following reaction (reaction *1* in Fig. 1):

$$CO_{2(g)} \leftrightarrow^{k_1} CO_{2(aq)}, \tag{1}$$

where k_1 is the rate coefficient of water-side mass transfer kinetics. Taking Eq. (1), the time dependence of the transient concentration of $CO_{2(aq)}$ can be calculated according to [36,37]:

$$\left[CO_{2(aq)}\right] = \left[CO^*_{2(aq)}\right]\left(1 - e^{-k_1 t}\right), \tag{2}$$

where t is the time, and $CO_{2(aq)}$ and $CO^*_{2(aq)}$ are the instantaneous and equilibrium CO_2 concentrations in the water phase, respectively. When CO_2 molecules are transferred from the gas phase (CO_2 bubble) to the water phase, they are able to take part in subsequent reactions (reactions *2* and *3* in Fig. 1), thus leading to the formation of H^+ and HCO_3^- as final products. These reactions can be represented by the following equations:

$$CO_{2(aq)} + H_2O \leftrightarrow^{K_2} H_2CO_3 \tag{3}$$

$$H_2CO_3 \leftrightarrow^{K_3} HCO_3^- + H^+ \tag{4}$$

where K_2 and K_3 are the equilibrium constants of the above two reactions.

As a result of the kinetic analysis performed for all interrelated reactions of the CO_2 hydration process in path (I) (Fig. 1), the final expression describing the change of H^+ concentration against time, as already mentioned above, adopted as a measure of the overall rate of this process, was found as:

$$[H^+]^2 = C_1\left(1 - e^{-k_1 t}\right) + C_2 \tag{5}$$

where C_1 and C_2 are fitting coefficients. The detailed derivation of this equation is provided in Appendix (A.2). According to this derivation, the coefficient C_1 is equal to the product of $CO^*_{2(aq)} \times K_2 \times K_3$, and hence, should be constant for a given temperature and CO_2 partial pressure. For 298 K and the CO_2 partial pressure of 1 bar, which corresponds to the conditions of the experiments, $C_1 = 1.50 \times 10^{-8}$ mol^2/L^2 (Appendix (A.2)). In turn, the coefficient C_2 is related to the initial concentration of H^+ ions and, if the experiment starts each time with the pure water, the value of this coefficient should also be constant. Assuming pH = 6.65, for t = 0, C_2 is approximately 5×10^{-14} mol^2/L^2 (Appendix (A.2)). Thus, as can be seen from the above analysis, while maintaining the same thermodynamic conditions for carrying out the CO_2 hydration process (C_1 and C_2 are constant) the only parameter determining its overall rate is the k_1 coefficient, which is related to the CO_2 transfer from the gas phase (CO_2 bubbles) to the water phase. By fitting the model to the experimental data, the rate coefficient k_1 can be determined. As discussed in detail in Appendix (A.2), higher k_1 values indicate a higher process rate, which means that the equilibrium state is reached faster.

An example of fitting Eq. (5) to the experimental data is shown in Fig. 6. This very good fit ($r^2 = 0.997$), with simultaneous obtaining the values of C_1 and C_2 coefficients very similar to the expected ones, confirms the correctness of the proposed model.

An equally good fit was obtained for all other measurements of pH change over time in the hydration process at different CO_2 flow rates, both for the inert mesh and the mesh with catalyst. The values of the k_1 coefficient obtained in this way are summarized in Table A.1, while the average values of k_1 from each measurement series are shown in Fig. 7a.

The first important conclusion resulting from Fig. 7a is that in the tested range of CO_2 flow rates, the k_1 value for a mesh covered with the Co_3O_4 film is always greater than in the case of an inert mesh. This confirms the catalytic nature of the former. It also clearly follows from

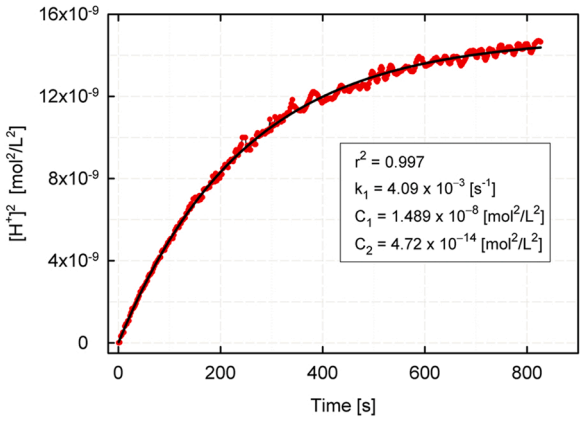

Fig. 6. An example of fitting Eq. (6) to experimental data for measuring CO_2 hydration (inert mesh, CO_2 flow rate – 170 mg/min). Points – experimental data, line – fitted Eq. (5).

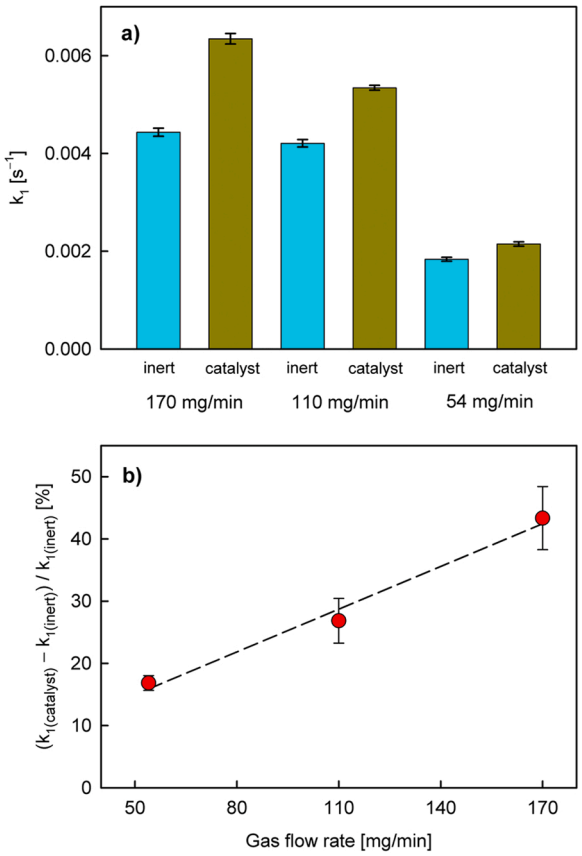

Fig. 7. (a) Average values of the rate coefficient of water-side mass transfer for the CO_2 hydration process at different CO_2 flow rates, both for the inert mesh and the mesh with catalyst. (b) Percentage increase in the k_1 value in the presence of the catalyst compared to its absence as a function of the CO_2 flow rate.

this that the catalyzed process is the process of CO_2 transfer from the gas phase to the phase constituting the surface of the catalyst. Thus, two parallel processes must be distinguished here: the "classical" transport of CO_2 from the surface of the bubbles or their parts that are in contact with the liquid phase, to this phase (uncatalyzed gas-liquid hydration path), as well as the CO_2 transport from the remaining parts of the bubble surfaces, which are in contact with the catalyst, to its surface (catalyzed gas-solid-liquid path). The efficiency of the catalytic process therefore depends on the ratio (A_{cat}/A_{total}) of the bubble surface areas involved in the CO_2 transport to the catalyst (A_{cat}) in relation to the total bubble surface areas (A_{total}).

Secondly, Fig. 7a shows that the increase in the CO_2 flow rate increases the k_1 value, which may be understandable (the contact area with the gas phase increases), however, the increase in k_1 for the mesh with catalyst is greater than for the inert mesh. This is illustrated in Fig. 7b. As can be seen, the higher the CO_2 flow rate, the greater the contribution of the catalytic process, which could indicate an increase in the A_{cat}/A_{total} ratio. A detailed analysis of the contact of bubbles with the mesh and their passage through it is such a complex problem [34,35] that in our case we cannot describe this process in a model way. However, it can be predicted [38], which is confirmed by the observations of our reactor (Fig. 3) during operation, that with the increase of the CO_2 flow rate, the bubbles coming out of the sparger are larger, leading to an increase in the A_{cat}/A_{total} ratio, thereby increasing the catalytic effect (the bubble contacts with a larger surface area of wire in the mesh). Over the measured range of CO_2 flow rate, the increase in the A_{cat}/A_{total} ratio is practically linear.

The above studies on the kinetics of the CO_2 hydration process showed the catalytic activity of plasma deposited thin films based on Co_3O_4 in the first step of this process, namely the transfer of CO_2 from the gas phase (bubble), which is enhanced by the solid phase (catalyst surface). Intriguing, however, that requires deeper explanations, is the nature and mechanism of the revealed catalytic process.

3.3. Molecular structure of the catalyst surface

To better understand the CO_2 hydration process taking place on the surface of the Co_3O_4-based catalyst, the molecular structure of this surface was investigated by XPS before and after contact with liquid water. These investigations were carried out as a function of the time of water exposure to the catalyst. Fig. 8 shows typical XPS core-level spectra of Co 2p, O 1 s, and C 1 s for the catalytic film before contact with liquid water (fresh sample) and, as an example, after 54 h of exposure to water.

The Co 2p spectrum was analyzed in the same way as in our previous papers [27,28]. This spectrum is spin-orbit splitted into a doublet: Co $2p_{3/2}$ and Co $2p_{1/2}$ bands, both revealing the same chemical surrounding of cobalt atoms. Therefore, only the more intense Co $2p_{3/2}$ band was examined and deconvoluted into three main asymmetric peaks assigned to Co^{3+} oxidation state at 779.5 eV, Co^{2+} oxidation state at 781.2 eV, and a satellite peak at approximately 788.4 eV. The ratio of the molar concentration of Co^{3+} to Co^{2+} states determined on this basis as a dependence on the treatment time with water is shown in Fig. 9. The value of the ratio for the fresh sample is very close to 2, which indicates the structure of the Co_3O_4 spinel. The relatively low intensity of the satellite peak and its binding energy of about 788 eV confirm the Co_3O_4 structure [39]. As can be seen, the Co^{3+}/Co^{2+} ratio is also practically equal to 2 (within the error limits) during the entire water treatment process, indicating no change in the oxidation state of the cobalt atoms in this process.

The analysis of the O 1 s spectrum was carried out by distinguishing three bands: the first (band *1*) at approx. 529.7 eV attributed to Co—O bonds (where oxygen is in the form of lattice O^{2-} atoms ($O_{lattice}$)) and the second (band *2*) at 531.0 – 531.15 eV assigned to Co—OH bonds [40–42], as well as the third (band *3*) band at about 532.5 eV, which corresponds to carbon—oxygen bonds [43]. The band *2* represents –OH groups derived from H_2O molecules, which are bound directly to Co atoms (OH_{Co}), as well as the groups formed on $O_{lattice}$ by H atoms cleaved from these H_2O molecules during their dissociation ($OH_{lattice}$) [42]. This band is also attributed to chemisorbed water in the form of H_2O clusters ($H_2O_{cluster}$). It has been reported that hydroxyl groups formed on Co atoms strongly anchor such clusters [40]. Unfortunately, the deconvolution of this band into a component related to –OH groups and a component derived from chemisorbed water clusters is not possible because their maxima are too close to each other and they overlap too accurately. Some information, however, can be provided by analyzing the position of the band *2* maximum. In Fig. 10, the positions of the bands *1*, *2* and *3* as a function of the treatment time with water are shown. As can be seen, only the band *2* is systematically shifted towards higher values, which can be interpreted as an increase in the intensity of the chemisorbed water component compared to the –OH component, because the former has the maximum at a slightly higher binding energy [44]. The positions of the other two bands have a statistical dispersion, with no systematic change with the time of exposure to water. The lack of such a change for the band *1* does not confirm the reported shift of this band towards higher energy with increasing water dose in the case of the model epitaxial Co_3O_4 layer (111), which has been interpreted as an increase of work function of the film surface due to the formation of hydroxyl groups [40]. This is probably the result of a much more complex Co_3O_4–based molecular structure in our case, in which any changes in surface potential caused by –OH groups are compensated by other interactions on such a surface. There is no doubt, however, that only in the case of –OH groups attached to the three-fold-coordinated Co^{2+} ions in the Co_3O_4 structure, properly formed potentials enable strong

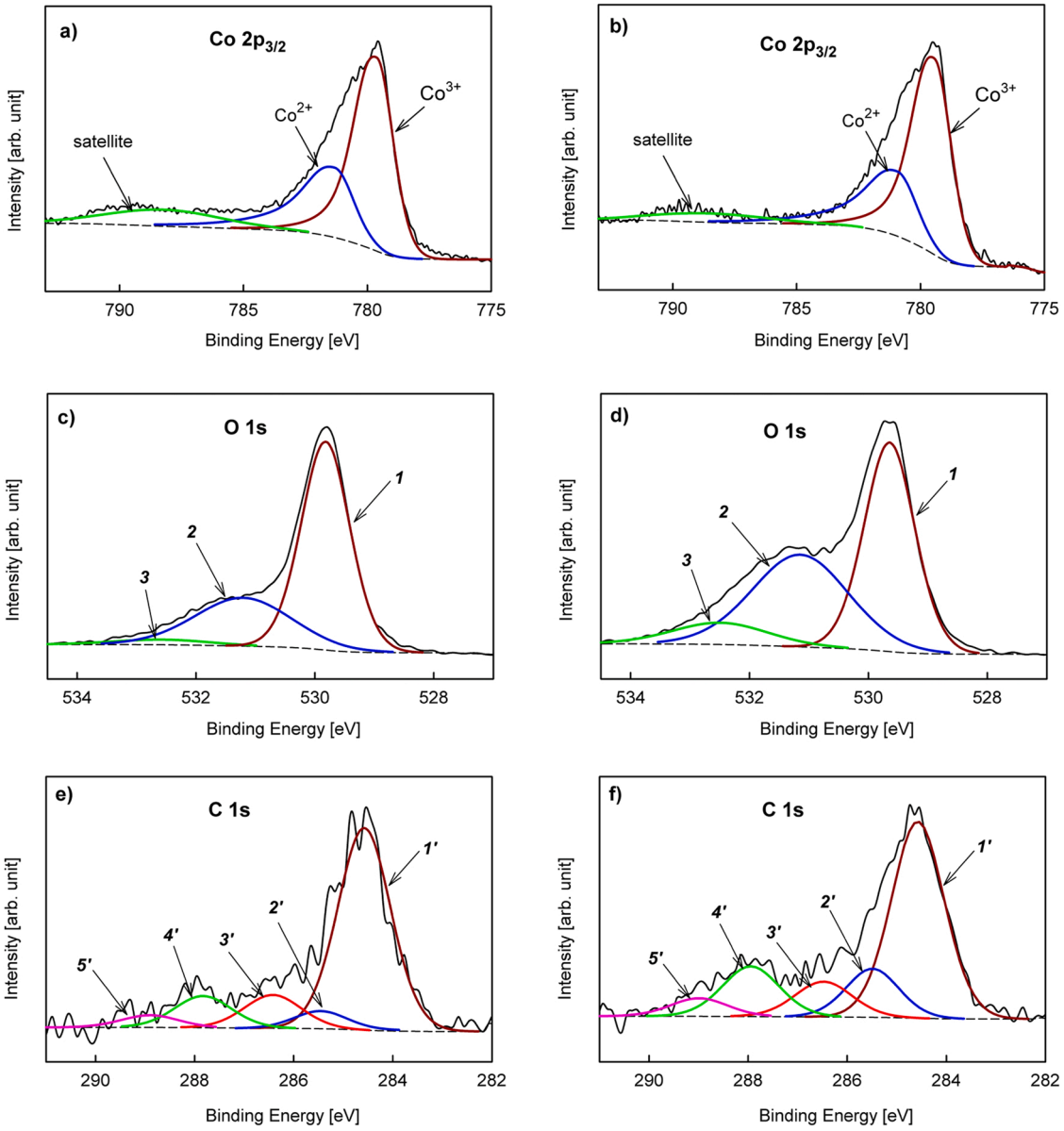

Fig. 8. Typical XPS core-level spectra of Co $2p_{3/2}$, O 1 s, and C 1 s for the Co_3O_4-based catalytic film. (a), (c), and (d) The film prior to contact with liquid water. (b), (d), and (f) The film after 54 h of exposure to liquid water. Band numbers: ***1*** - Co−O; ***2*** - Co−OH; ***3*** - C−O, C═O; ***1'*** - C═C; ***2'*** - C−C, C-H; ***3'*** - C−OH, C−O−C; ***4'*** - C═O; ***5'*** - O−C═O.

anchoring of H_2O clusters [40].

The broad and relatively weak band *3* in the spectrum O 1 s includes organic combinations of carbon with oxygen, both C−O and C═O, which, however, in such a complex system as the investigated one, cannot be distinguished. The C 1 s spectra shown in Figs. 8e and 8f can be helpful in this analysis. According to the literature [43,45], the spectra have been deconvoluted into five bands. Three of them are attributed to organic carbon−oxygen combinations: band *3'* at 286.3 – 286.5 eV is assigned to C−OH and C−O−C, band 4' at 287.8 – 289.0 eV to C═O, and band *5'* at about 289 eV is linked to O−C═O structures. Apart from the carbon−oxygen species, the C 1 s spectra also show distinct bands for C−C or C−H (sp^3) and C═C (sp^2) at 284.6 eV (band *1'*) and 285.5 eV (band *2'*), respectively. These carbon forms will be discussed later in the paper.

From the point of view of the CO_2 hydration process, the hydroxyl groups formed on the surface of Co_3O_4 nanocrystallites, as well as water molecules strongly chemisorbed on them in the form of H_2O clusters, are of particular importance. In the simple approach, taking into account, above all, the three-fold-coordinated Co^{2+} ions [40], the formation of hydroxyl groups can be schematically represented, as in Fig. 11.

In the first step, a H_2O molecule attaches to the Co^{2+} ion, and then it dissociates into the −OH group and atomic H. The hydrogen atom can combine with the lattice oxygen O^{2-} to form another −OH group (scheme (a)). The second hydrogen atom from the originally attached water molecule can also dissociate and form the next −OH group with the lattice oxygen (scheme (b)) [42]. In each of these cases the number of −OH groups increases twice as fast as the number of "free" lattice oxygen atoms ($O_{lattice}$) decreases. In a situation where the hydrogen atoms can be bonded in the material in a way other than only to the lattice oxygen, for example to carbon atoms, the number of "free" $O_{lattice}$ may remain unchanged with a simultaneous increase in the number of −OH groups (scheme (c)), or the number of "free" $O_{lattice}$ can increase without increasing the number of −OH groups (scheme (d)). It is obvious that all these four processes can occur simultaneously but at different efficiency.

Bearing in mind the presented reaction schemes (Fig. 11), we

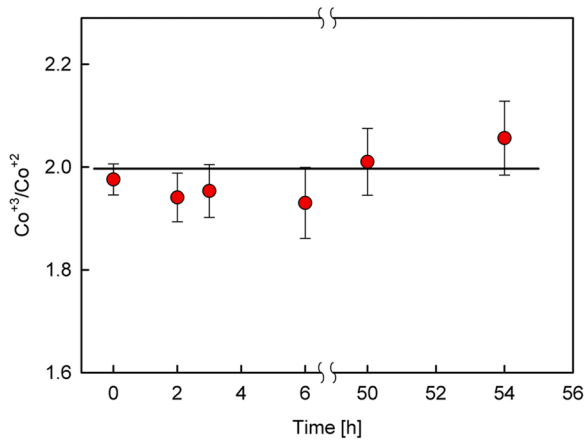

Fig. 9. The ratio of the molar concentration of Co^{3+} to Co^{2+} as a function of the treatment time with liquid water.

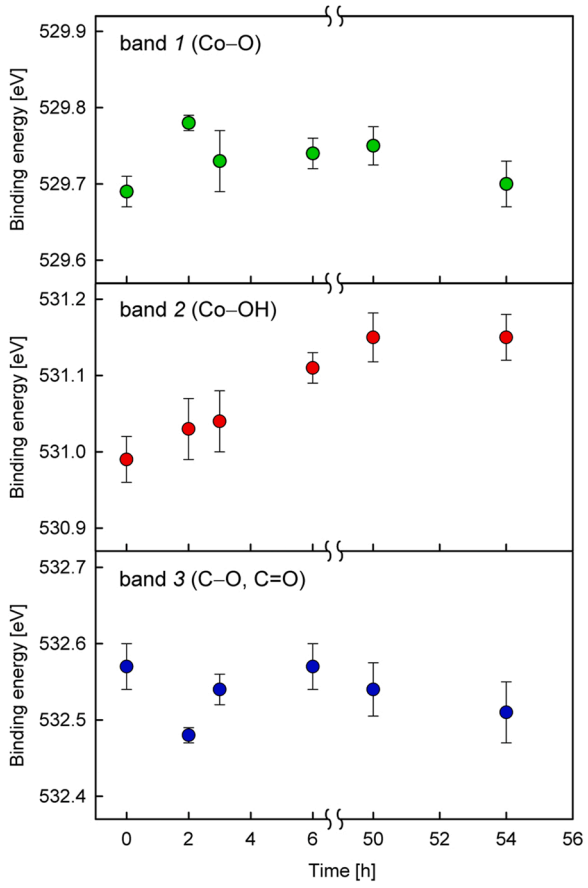

Fig. 10. Position of the maxima of bands *1*, *2*, and *3* (shown in Fig. 8c and d) as a function of the treatment time with liquid water.

analyzed the change in $O_{lattice}$ density as a function of the treatment time with liquid water, based on the band *1* from the XPS O 1 s spectrum (Figs. 8c and 8d). Such a dependence is shown in Fig. 12a. It should be added that the density of a given species (in this case $O_{lattice}$) is understood as the relative density calculated in relation to the content of all Co atoms. The concept of density defined in this way will be used in the rest of the paper. As can be seen, the density of $O_{lattice}$ increases with the treatment time with water, aiming to achieve a constant value. Assume that after 54 h the value corresponding to the $O_{lattice}$/Co ratio is equal to the theoretical value $4/3 = 1.33$ (Co_3O_4). Thus, we can estimate the

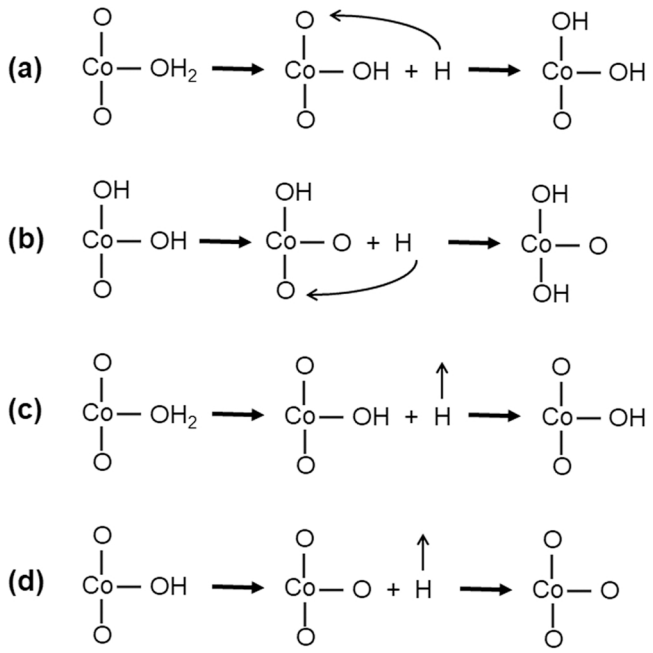

Fig. 11. Proposed mechanism of the formation of hydroxyl groups on the surface of the Co_3O_4 structure with the participation of Co^{2+} ions.

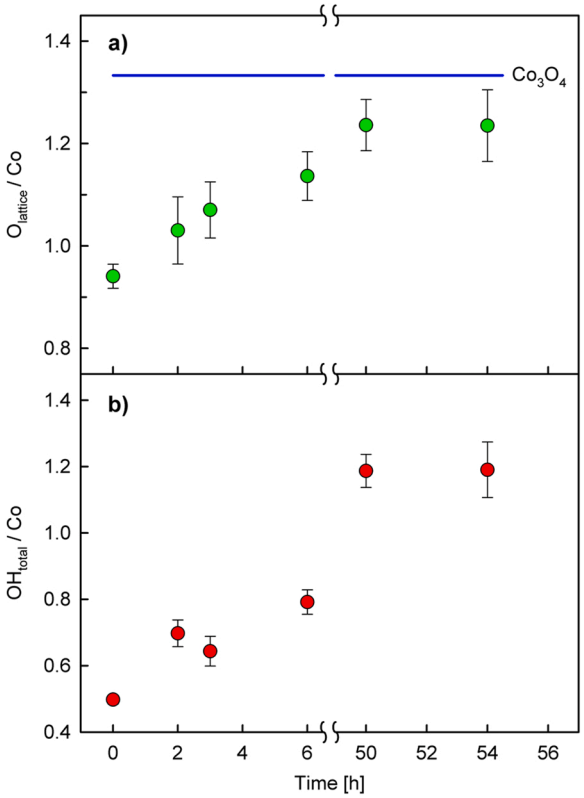

Fig. 12. Density of oxygen-based species calculated from the XPS O 1 s spectrum bands (Fig. 8c and d) as a function of the treatment time with liquid water. (a) The relative density of $O_{lattice}$ based on the band *1* (Co–O). (b) The relative density of OH_{total} based on the band *2* (Co–OH).

$O_{lattice}$ density involved in the formation of –OH groups, which is around 0.1. This is the difference between the value of 1.33 and the measured $O_{lattice}$ density for the time of 54 h (the lattice oxygen involved in the formation of the –OH group is not visible in band *1* of the O 1 s

spectrum). There is no doubt that the density of −OH groups formed on $O_{lattice}$ ($OH_{lattice}$) increases (certainly does not decrease) with the treatment time with liquid water, so the determined value of the density of $OH_{lattice}$ groups can be considered as the maximum density of such groups in the investigated catalytic film. However, if this is the case, the density of $O_{lattice}$ in the film prior to its contact with liquid water is clearly less than the theoretical value of 1.33. It is approximately 0.95 (for time t = 0). Even if we assume that all the $OH_{lattice}$ groups identified after 54 h in liquid water were previously formed as a result of contact with water in the air, and therefore are already present at time t = 0, the total $O_{lattice}$ density will be only 1.05 (0.95 + 0.1). This proves that the spinel structure is highly defected and there is a high density of vacancies associated with the absence of $O_{lattice}$. This density is at least about 0.3 vacancy/Co. The increase in the $O_{lattice}$ density with the time of treatment with liquid water indicates that the vacancies are systematically filled with oxygen atoms, according to the scheme (d) (Fig. 11).

In turn, the change in the density of species assigned to the band *2* in the O 1 s spectrum (together called OH_{total}) as a function of the water exposure time is shown in Fig. 12b. These are −OH groups attached to Co^{2+} atoms in the direct reaction with water molecules (OH_{Co}), −OH groups formed on $O_{lattice}$ ($OH_{lattice}$), and strongly chemisorbed water molecules ($H_2O_{cluster}$). The complexity of this band, as already mentioned, does not allow the quantification of the ratio between the contents of these individuals to be established. However, we can estimate the predicted maximum density of −OH groups (OH_{Co} + $OH_{lattice}$). If we assume that after 54 h of exposure to water, a single −OH group from direct reaction with H_2O is attached to each Co^{2+} atom, then their relative density will be $OH_{Co}Co$ = 0.33 (since Co^{2+}/Co in Co_3O_4 is 0.33). After the same time, the density of the $OH_{lattice}$ groups is about 0.1, as it was shown above. Thus, the density of the −OH groups will be at most 0.43, which is significantly lower than the measured value of about 1.2 (Fig. 12b). This result confirms the presence of a significant number of chemisorbed H_2O clusters, which are most likely attached, as mentioned earlier, to the OH_{Co} groups.

The implementation of processes (c) and (d) (Fig. 11) requires the attachment of hydrogen atoms in a different way than to $O_{lattice}$ atoms. It can be assumed that the carbon fraction plays an important role in this case. This fraction constitutes about 14 at% of the catalytic film (from the XPS measurements). Comparison of the C 1 s spectra for the catalytic film before contact with liquid water and after 54 h of exposure to water (Figs. 8e and 8f) shows a significant increase in the content of (C—H + C—C) bonds (band *2'*) compared to the content of C=C bonds (band *1'*). Changes in the content of these bonds in relation to the total number of carbon atoms are presented in Figs. 13a and 13b as a function of the exposure time to water. The increase in the (C—H + C—C) content with a simultaneous decrease in the C=C content can be attributed to the saturation of double bonds in the reaction with hydrogen atoms released in processes (c) and (d). However, the direct reaction of H_2O molecules with double bonds of the carbon matrix should also be taken into account, as indicated by the systematic increase in the number of C—O bonds (most probably as C—OH) in relation to the carbon content (Fig. 13c). The proton released during dissociation of these H_2O molecules can also be attached to double bonds of the carbon fraction. The contents of other organic carbon-oxygen combinations (bands 4 'and 5' in Figs. 8e and 8f) remain constant within the error limits during the water treatment process.

Analogous XPS studies were also carried out for the molecular structure of the Co_3O_4-based catalyst surface being in contact with liquid water and bubbled CO_2. The obtained XPS spectra did not differ from the spectra discussed above for the catalyst contacted only with pure water. These results indicate that CO_2 does not induce any permanent changes on the catalyst surface.

3.4. Proposed mechanism of the catalytic activity

When trying to elucidate the mechanism of the revealed catalytic

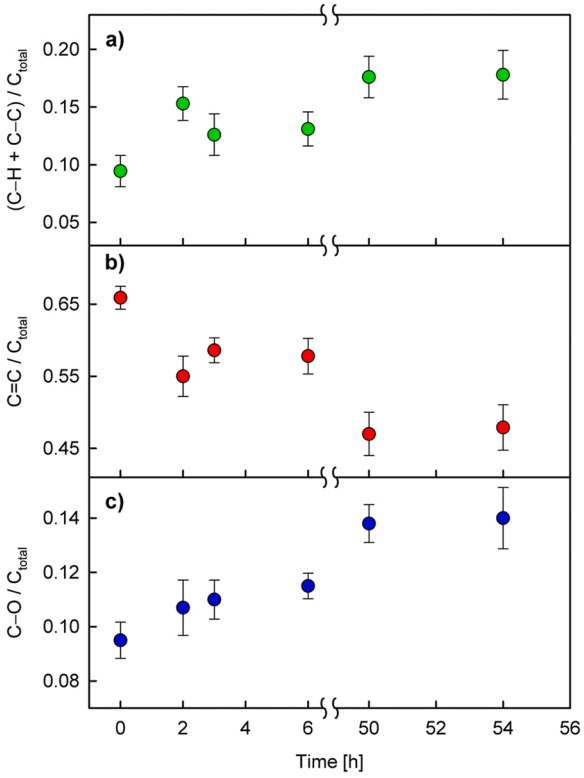

Fig. 13. Density of carbon-based species calculated from the XPS C 1 s spectrum bands (Fig. 8e and f) as a function of the treatment time with liquid water. (a) The relative density of (C−H + C−C) based on the band *2'*. (b) The relative density of C=C based on the band *1'*. (c) The relative density of C−O based on the band *3'*.

influence of Co_3O_4-based thin films on the CO_2 hydration, two key experimental facts should be taken into account. First, the kinetic analysis showing that the catalytic effect is related to the gas-liquid mass transfer, which suggests that the catalytic reaction occurs at the interface of the CO_2 bubble and the catalyst, and secondly, the study of the molecular structure of the catalyst surface, which indicates the presence of water clusters. The contact area of the CO_2 bubble and the catalyst is however small compared to the total surface area of the bubble. Thus, two parallel processes take place here: the "extracting" of CO_2 molecules by the active catalyst surface and the "classical" CO_2 transfer from the remaining bubble surface into the liquid phase. Therefore, in the catalyzed CO_2 hydration, the products of this process in the form of H^+ and HCO_3^- ions are virtually produced via two pathways: in the reaction of dissolved $CO_{2(aq)}$ with H_2O (path (I) in Fig. 1) and in the direct reaction of gaseous CO_2 (in the area where the bubbles come into contact with the catalyst surface) with the H_2O clusters on this surface.

The role played in the CO_2 hydration process by adsorbed water−metal oxide interfaces has been discussed several times on the basis of both experimental studies and quantum-chemical calculations. Already over 30 years ago it was calculated that in a pure solution of CO_2 in water, the reaction of two H_2O molecules with CO_2 is much more favorable than the reaction with one H_2O molecule [46]. This conclusion was used when interpreting the results confirming the formation of bicarbonate on the TiO_2 surface [47]. Subsequent studies carried out on Fe_2O_3 and γ-Al_2O_3 (in contact with the gas phase) confirmed the significant participation in the CO_2 hydration process of both −OH groups present on the surface of these oxides and adsorbed water molecules (forming a thin film with a thickness of a couple of monolayers). It was found that in the absence of adsorbed water, CO_2 reacts with surface −OH groups to form adsorbed bicarbonate on the surface. In the presence of adsorbed water, this reaction is blocked as water hydrogen

bonds to the reactive M−OH sites. Instead, CO_2 reacts with adsorbed water to yield adsorbed carbonate and protonated surface hydroxyl groups, $M-OH_2^+$, through a proposed H_2CO_3 intermediate [48,49]. In the case of contact of the metal oxide surfaces with the liquid phase, we can expect a rapid desorption of H^+ and HCO_3^- ions into the solution.

More sophisticated analysis performed by the quantum chemical calculations for neutral hydration of CO_2 showed that in this chemical process water molecules actively participate as a catalyst [50–53]. In aqueous solution the hydration mechanism is multimolecular, where geometric parameters of the solvent fully intervene in the reaction coordinate. The hydration process was found to proceed through an attack of a water oxygen to the CO_2 carbon in concert with a proton transfer to a CO_2 oxygen. The proton transfer is assisted by a chain of water molecules, which is necessary for a proton relay between different oxygens. The calculated results showed the direct participation of a cluster of three water molecules as most likely to be actively involved in the neutral hydration of CO_2 in aqueous solution. The activation barrier of the H_2CO_3 formation decreases in magnitude with the number of H_2O molecules in the cluster and in the case of three H_2O molecules it is about 60% lower with respect to the one water molecule reaction [50, 51]. The analysis carried out under similar computational conditions, assuming the presence of $Al(OH)_3$, i.e. the system that can be considered as a M−OH model, showed that the activation barrier in the reaction between CO_2 molecules and H_2O clusters coordinated to $Al(OH)_3$ was much less than that for analogous clusters in the absence of $Al(OH)_3$ [52]. This undoubtedly confirms the belief that the formation of H_2O clusters on the M−OH surface constitutes catalytic centers for the hydration process. Subsequent quantum-chemical calculations performed for the MgO surface showed that water molecules could also dissociate into H^+ and OH^- ions. The formation of the dissociated ions is strongly related to the presence of coadsorbed water molecules to allow the formation of hydrogen bonds. The adsorption of a single water molecule does not lead to dissociation. For the dimer and trimer of water molecules, one molecule dissociates while the others coadsorbed stabilize the H^+ and OH^- ionic species on the surface [53]. The presence of OH^- ions can certainly also accelerate the hydration process in accordance with the path II (Fig. 1).

The concept of hydroxyl groups formed on metal atoms with strongly anchored water clusters ($M-OH(nH_2O)$) is especially well suited to our results. Fig. 14 shows a scheme presenting the proposed process of catalytic CO_2 hydration towards bicarbonate on the Co_3O_4-based thin films.

In our discussion on the catalytic activity mechanism, two parallel processes should be kept in mind: the "classical" transport of CO_2 from the bubbles to the liquid phase (non-catalyzed gas-liquid hydration path) and the catalyzed gas-solid-liquid path, involving in the first stage the transport of CO_2 from the bubble surface to the catalyst surface (see Section 3.2). Thus, during the hydration of CO_2 in the presence of a catalytic film, reaction products, including H^+ and HCO_3^- ions, are formed via two pathways: (i) uncatalyzed CO_2 hydration and (ii) catalyzed CO_2 gas hydration with chemisorbed H_2O clusters onto the catalyst surface. The small geometric area of the contact between CO_2 bubbles and the catalyst surface in relation to the direct gas-liquid contact area, explains why the observed catalytic effect is not very large, but it is certainly visible. The fitted values of the parameter k_1 for the experiments with the catalyst are systematically higher than the corresponding values for the inert support under the same hydrodynamic conditions, which proves the catalytic activity of the plasma-prepared Co_3O_4 films.

4. Conclusions

The experimental studies of the CO_2 hydration process presented in this paper, supported by the proposed kinetic model, which fits the obtained results very well, have shown that the bottleneck of the entire process is its first step, i.e. the transfer of CO_2 from the gas phase to the liquid phase. The subsequent reactions of dissolved CO_2 with H_2O molecules, which lead to products in the form of H^+ and HCO_3^- (Fig. 1) are significantly faster. Thus, looking for opportunities to catalytically accelerate the hydration process, one should focus primarily on the CO_2 mass transfer step. With this approach in mind, we concentrated our research on inorganic heterogeneous catalysts that could accelerate the CO_2 hydration process, opening up a new possibility involving the transfer of CO_2 from the gas phase (bubble) to the solid phase (catalyst surface), and then the final products of CO_2-H_2O reaction to the liquid phase. It was found that thin films based on Co_3O_4 plasma deposited on the wire mesh perform well as such a catalyst. The study of the molecular structure of this catalyst has shown that chemisorbed H_2O clusters attached to −OH groups, which are bonded to Co^{2+} ions in the Co_3O_4 lattice, are located on its surface. The interaction of these clusters with CO_2 molecules in the gas phase accelerates the overall hydration process.

In the tested experimental setup, at room temperature and a CO_2 flow rate of 170 g/min, the rate of the CO_2 hydration process was about 40% faster for the Co_3O_4 coated mesh than for the inert mesh. It should be emphasized, however, that the hydration process by the route: gas phase - solid phase - liquid phase, takes place only to a small extent compared to its occurrence through the direct route: gas phase - liquid phase. The proportion of bubble surface area which is in contact with the catalyst to the total bubble surface area (A_{cat}/A_{total}) is extremely small, especially since the catalyst surface is highly hydrophilic (water contact angle is about 8°). Based on this knowledge, we can propose further work aimed at intensifying the increase in the rate of the hydration process using the plasma-deposited thin-film catalyst based on Co_3O_4. These efforts should focus primarily on designing an appropriate structured packing for bubble reactors, ensuring a much greater contact

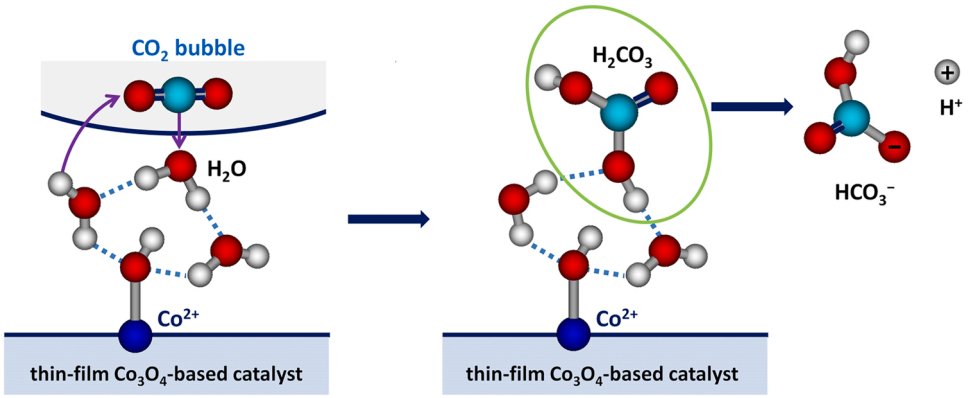

Fig. 14. Scheme of the proposed CO_2 hydration process catalyzed by the plasma-deposited Co_3O_4-based thin film.

of the gas phase with the catalyst surface. Research should also be undertaken on increasing the hydrophobicity of the catalytic film surface, for example by designing and preparing an appropriate nanostructure of the surface using the plasma treatment process.

It should also be noted, that demonstrating the original catalytic mechanism for our plasma-deposited thin films based on Co_3O_4 opens up opportunities for new searches for other similarly acting, perhaps better, inorganic catalysts for the CO_2 hydration process.

CRediT authorship contribution statement

Hanna Kierzkowska-Pawlak: Conceptualization, Methodology, Manuscript writing **Ewelina Kruszczak:** Investigation, Data curation. **Jacek Tyczkowski:** Conceptualization, Supervision, Manuscript writing.

Declaration of Competing Interest

The authors declare that they have no known competing financial interests or personal relationships that could have appeared to influence the work reported in this paper.

Acknowledgments

This work was financially supported by the National Science Centre (NCN) of Poland (Dec. 2017/25/B/ST8/00969). The authors thank M. Sc. R. Kapica for support during plasma deposition of thin films and Dr. J. Balcerzak for performing XPS measurements.

Appendix A. Supporting information

Supplementary data associated with this article can be found in the online version at doi:10.1016/j.apcatb.2021.120961.

References

[1] F. Zeng, C. Mebrahtu, X. Xi, L. Liao, J. Ren, J. Xie, H.J. Heeres, R. Palkovits, Catalysts design for higher alcohols synthesis by CO_2 hydrogenation: trends and future perspectives, Appl. Catal. B 120073 (2021), https://doi.org/10.1016/j.apcatb.2021.120073.

[2] I. Ghiat, T. Al-Ansari, A review of carbon capture and utilisation as a CO_2 abatement opportunity within the EWF nexus, J. CO2 Util. 45 (2021), 101432, https://doi.org/10.1016/j.jcou.2020.101432.

[3] M. Liu, T. Peng, H. Li, L. Zhao, Y. Sang, Q. Feng, l Xu, Y. Jiang, H. Liu, J. Zhang, Photoresponsive nanostructure assisted green synthesis of organics and polymers, Appl. Catal. B 249 (2019) 172–210, https://doi.org/10.1016/j.apcatb.2019.02.071.

[4] P.H.M. Feron, Absorption-Based Post-Combustion Capture of Carbon Dioxide, Woodhead Publishing, Amsterdam, 2016, https://doi.org/10.1016/C2014-0-03382-5.

[5] K. Kunze, G. Dojchinov, V.S. Haritos, P. Lutze, Reactive absorption of CO_2 into enzyme accelerated solvents: from laboratory to pilot scale, Appl. Energy 156 (2015) 676–685, https://doi.org/10.1016/j.apenergy.2015.07.033.

[6] R.A. Kelsey, D.A. Miller, S.R. Parkin, K. Liu, J.E. Remias, Y. Yang, F.C. Lightstone, K. Liu, C.A. Lippert, S.A. Odom, Carbonic anhydrase mimics for enhanced CO_2 absorption in an amine-based capture solvent, Dalton Trans. 45 (1) (2016) 324–333, https://doi.org/10.1039/C5DT02943K.

[7] P. Mirjafari, K. Asghari, N. Mahinpey, Investigating the application of enzyme carbonic anhydrase for CO_2 sequestration purposes, Ind. Eng. Chem. Res. 46 (3) (2007) 921–926, https://doi.org/10.1021/ie060287u.

[8] X. Wang, W. Conway, R. Burns, N. McCann, M. Maeder, Comprehensive study of the hydration and dehydration reactions of carbon dioxide in aqueous solution, J. Phys. Chem. A 114 (4) (2009) 1734–1740, https://doi.org/10.1021/jp909019u.

[9] M.J. Mitchell, O.E. Jensen, K.A. Cliffeand, M.M. Maroto-Valer, A model of carbon dioxide dissolution and mineral carbonation kinetics, Proc. R. Soc. A 466 (2010) 1265–1290, https://doi.org/10.1098/rspa.2009.0349.

[10] G.A. Bhaduri, M.A. Alamiry, L. Šiller, Nickel nanoparticles for enhancing carbon capture, J. Nanomater. 16 (1) (2015) 376, https://doi.org/10.1155/2015/581785.

[11] D.T. Phan, M. Maeder, R.C. Burns, G. Puxty, Catalysis of CO_2 absorption in aqueous solution by inorganic oxoanions and their application to post combustion capture, Environ. Sci. Technol. 48 (8) (2014) 4623–4629, https://doi.org/10.1021/es500667s.

[12] D.T. Phan, M. Maeder, R.C. Burns, G. Puxty, Catalysis of CO_2 absorption in aqueous solution by vanadate and sulfate and their application to post combustion capture, Int. J. Greenh. Gas Control 36 (2015) 60–65, https://doi.org/10.1016/j.ijggc.2015.02.013.

[13] G. Hu, N.J. Nicholas, K.H. Smith, K.A. Mumford, S.E. Kentish, G.W. Stevens, Carbon dioxide absorption into promoted potassium carbonate solutions: a review, Int. J. Greenh. Gas Control 53 (2016) 28–40, https://doi.org/10.1016/j.ijggc.2016.07.020.

[14] T. Sharma, S. Sharma, H. Kamyab, A. Kumar, Energizing the CO_2 utilization by chemo-enzymatic approaches and potentiality of carbonic anhydrases: a review, J. Clean. Prod. 247 (2020), 119138, https://doi.org/10.1016/j.jclepro.2019.119138.

[15] B. Morreale, F. Shi, Novel Materials for Carbon Dioxide Mitigation Technology, Elsevier, Amsterdam, 2015, https://doi.org/10.1016/C2012-0-01304-X.

[16] J.K. Yong, G.W. Stevens, F. Caruso, S.E. Kentish, The use of carbonic anhydrase to accelerate carbon dioxide capture processes, J. Chem. Technol. Biotechnol. 90 (1) (2015) 3–10, https://doi.org/10.1002/jctb.4502.

[17] B.H. Jo, J.H. Seo, Y.J. Yang, K. Baek, Y.S. Choi, S.P. Pack, S.H. Oh, H.J. Cha, Bioinspired silica nanocomposite with autoencapsulated carbonic anhydrase as a robust biocatalyst for CO_2 sequestration, ACS Catal. 4 (12) (2014) 4332–4340, https://doi.org/10.1021/cs5008409.

[18] C.A. Lippert, K. Liu, M. Sarma, S.R. Parkin, J.E. Remias, C.M. Brandewie, S. A. Odomand, K. Liu, Improving carbon capture from power plant emissions with zinc-and cobalt-based catalysts, Catal. Sci. Technol. 4 (10) (2014) 3620–3625, https://doi.org/10.1039/C4CY00766B.

[19] J.G. Rains, K. O'Donnelly, T. Oliver, R. Woscholski, N.J. Longand, L.M. Barter, Bicarbonate inhibition of carbonic anhydrase mimics hinders catalytic efficiency: elucidating the mechanism and gaining insight toward improving speed and efficiency, ACS Catal. 9 (2) (2019) 1353–1365, https://doi.org/10.1021/acscatal.8b04077.

[20] G.A. Bhaduri, L. Šiller, Nickel nanoparticles catalyse reversible hydration of carbon dioxide for mineralization carbon capture and storage, Catal. Sci. Technol. 3 (5) (2013) 1234–1239, https://doi.org/10.1039/C3CY20791A.

[21] D. Britt, Comment on "Nickel nanoparticles catalyse reversible hydration of carbon dioxide for mineralization carbon capture and storage" by G. Bhaduri and L. Šiller, Catal. Sci. Technol. 3 (9) (2013) 2195–2196, https://doi.org/10.1039/C3CY00357D, 1234.

[22] J.J. Ramsden, I.J. Sokolov, D.J. Malik, Questioning the catalytic effect of Ni nanoparticles on CO_2 hydration and the very need of such catalysis for CO_2 capture by mineralization from aqueous solution, Chem. Eng. Sci. 175 (2018) 162–167, https://doi.org/10.1016/j.ces.2017.09.042.

[23] W. Yu, T. Wang, A.H.A. Park, M. Fang, Review of liquid nano-absorbents for enhanced CO_2 capture, Nanoscale 11 (37) (2019) 17137–17156, https://doi.org/10.1039/C9NR05089B.

[24] S.Y. Cheng, Y.Z. Liu, G.S. Qi, Progress in the enhancement of gas–liquid mass transfer by porous nanoparticle nanofluids, J. Mater. Sci. 54 (2019) 13029–13044, https://doi.org/10.1007/s10853-019-03809-w.

[25] J. Tyczkowski, Cold plasma produced catalytic materials, in: T. Mieno (Ed.), Plasma Science and Technology - Progress in Physical States and Chemical Reactions, InTech, Rijeka, 2016, pp. 25–65, https://doi.org/doi:10.5772/60692.

[26] Z. Wang, Y. Zhang, E.C. Neyts, X. Cao, X. Zhang, B.W.L. Jang, C.J. Liu, ACS Catal. 8 (2018) 2093–2110, https://doi.org/10.1021/acscatal.7b03723.

[27] J. Tyczkowski, H. Kierzkowska-Pawlak, R. Kapica, J. Balcerzak, J. Sielski, Cold plasma – a promising tool for the production of thin-film nanocatalysts, Catal. Today 337 (2019) 44–54, https://doi.org/10.1016/j.cattod.2019.03.037.

[28] H. Kierzkowska-Pawlak, J. Tyczkowski, J. Balcerzak, P. Tracz, Advances in plasma produced CoOX-based nanocatalysts for CO_2 methanation, Catal. Today 337 (2019) 162–170, https://doi.org/10.1016/j.cattod.2019.04.035.

[29] X. Deng, H. Tüysüz, Cobalt-oxide-based materials as water oxidation catalyst: recent progress and challenges, ACS Catal. 4 (2014) 3701–3714, https://doi.org/10.1021/cs500713d.

[30] J. Łojewska, A. Kołodziej, T. Łojewski, R. Kapica, J. Tyczkowski, Structured cobalt oxide catalyst for VOC combustion. Part I: Catalytic and engineering correlations, Appl. Catal. A Gen. 366 (1) (2009) 206–211, https://doi.org/10.1016/j.apcata.2009.07.006.

[31] C. Badini, F. Laurella, Oxidation of FeCrAl alloy: influence of temperature and atmosphere on scale growth rate and mechanism, Surf. Coat. Technol. 135 (2–3) (2001) 291–298, https://doi.org/10.1016/S0257-8972(00)00989-0.

[32] G.M. Bond, J. Stringer, D.K. Brandvold, F.A. Simsek, M.G. Medina, G. Egeland, Development of integrated system for biomimetic CO_2 sequestration using the enzyme carbonic anhydrase, Energy Fuels 15 (2) (2001) 309–316, https://doi.org/10.1021/ef000246p.

[33] D.H. Kim, M. Vinoba, W.S. Shin, K.S. Lim, S.K. Jeong, S.H. Kim, Biomimetic sequestration of carbon dioxide using an enzyme extracted from oyster shell, Korean J. Chem. Eng. 28 (10) (2011) 2081, https://doi.org/10.1007/s11814-011-0071-z.

[34] J. Yong, F. Chen, W. Li, J. Huo, Y. Fang, Q. Yang, H. Bian, X. Hou, Underwater superaerophobic and superaerophilic nanoneedles-structured meshes for water/bubbles separation: removing or collecting gas bubbles in water, Glob. Chall. 2 (4) (2018), 1700133, https://doi.org/10.1002/gch2.201700133.

[35] J. Park, J. Ryu, S.J. Lee, Penetration of a bubble through porous membranes with different wettabilities, Soft Matter 15 (29) (2019) 5819–5826, https://doi.org/10.1039/C9SM00754G.

[36] J. Benitez. Principles and Modern Applications of Mass Transfer Operations, third ed., John Wiley & Sons, Hoboken, New Jersey, 2016.

[37] K. Liu, J.R. Phillips, X. Sun, S. Mohammad, R.L. Huhnke, H.K. Atiyeh, Investigation and modeling of gas-liquid mass transfer in a sparged and non-sparged continuous

stirred tank reactor with potential application in syngas fermentation, Fermentation 5 (3) (2019) 75, https://doi.org/10.3390/fermentation5030075.
[38] H. Mirsandi, W.J. Smit, G. Kong, M.W. Baltussen, E.A.J.F. Peters, J.A.M. Kuipers, Influence of wetting conditions on bubble formation from a submerged orifice, Exp. Fluids 61 (3) (2020) 1–18, https://doi.org/10.1007/s00348-020-2919-7.
[39] S.C. Petitto, E.M. Marsh, G.A. Carson, M.A. Langell, Cobalt oxide surface chemistry: the interaction of CoO (100), Co_3O_4 (110) and Co_3O_4 (111) with oxygen and water, J. Mol. Catal. A Chem. 281 (1–2) (2008) 49–58, https://doi.org/10.1016/j.molcata.2007.08.023.
[40] M. Schwarz, F. Faisal, S. Mohr, C. Hohner, K. Werner, T. Xu, T. Skala, N. Tsud, K. C. Prince, V. Matolin, Y. Lykhach, J. Libuda, Structure-dependent dissociation of water on cobalt oxide, J. Phys. Chem. Lett. 9 (11) (2018) 2763–2769, https://doi.org/10.1021/acs.jpclett.8b01033.
[41] Z. Chen, C.X. Kronawitter, I. Waluyo, B.E. Koel, Investigation of water dissociation and surface hydroxyl stability on pure and Ni-modified CoOOH by ambient pressure photoelectron spectroscopy, J. Phys. Chem. B 122 (2) (2018) 810–817, https://doi.org/10.1021/acs.jpcb.7b06960.
[42] J. Fester, M. García-Melchor, A.S. Walton, M. Bajdich, Z. Li, L. Lammich, A. Vojvodic, J.V. Lauritsen, Edge reactivity and water-assisted dissociation on cobalt oxide nanoislands, Nat. Commun. 8 (2017) 14169, https://doi.org/10.1038/ncomms14169.
[43] G. Beamson, D. Briggs. High Resolution XPS of Organic Polymers: The Scienta ESCA300 Database, first ed., Wiley, New York, 1992.
[44] X. Deng, T. Herranz, C. Weis, H. Bluhm, M. Salmeron, Adsorption of water on Cu_2O and Al_2O_3 thin films, J. Phys. Chem. C 112 (26) (2008) 9668–9672, https://doi.org/10.1021/jp800944r.
[45] J. Diaz, G. Paolicelli, S. Ferrer, F. Comin, Separation of the sp^3 and sp^2 components in the C1s photoemission spectra of amorphous carbon films, Phys. Rev. B 54 (11) (1996) 8064–8069, https://doi.org/10.1103/PhysRevB.54.8064.
[46] K.M. Merz Jr, Gas-phase and solution-phase potential energy surfaces for carbon dioxide+ n-water (n= 1, 2), J. Am. Chem. Soc. 112 (22) (1990) 7973–7980, https://doi.org/10.1021/ja00178a019.
[47] M.A. Henderson, Evidence for bicarbonate formation on vacuum annealed TiO_2 (110) resulting from a precursor-mediated interaction between CO_2 and H_2O, Surf. Sci. 400 (1–3) (1998) 203–219, https://doi.org/10.1016/S0039-6028(97)00863-7.
[48] J. Baltrusaitis, V.H. Grassian, Surface reactions of carbon dioxide at the adsorbed water−iron oxide interface, J. Phys. Chem. B 109 (25) (2005) 12227–12230, https://doi.org/10.1021/jp051868k.
[49] J. Baltrusaitis, J.D. Schuttlefield, E. Zeitler, J.H. Jensen, V.H. Grassian, Surface reactions of carbon dioxide at the adsorbed water−oxide interface, J. Phys. Chem. C 111 (40) (2007) 14870–14880, https://doi.org/10.1021/jp0746771.
[50] M.T. Nguyen, G. Raspoet, L.G. Vanquickenborne, P.T.Van Duijnen, How many water molecules are actively involved in the neutral hydration of carbon dioxide? J. Phys. Chem. A 101 (40) (1997) 7379–7388, https://doi.org/10.1021/jp9701045.
[51] M.T. Nguyen, M.H. Matus, V.E. Jackson, V.T. Ngan, J.R. Rustad, D.A. Dixon, Mechanism of the hydration of carbon dioxide: direct participation of H_2O versus microsolvation, J. Phys. Chem. A 112 (41) (2008) 10386–10398, https://doi.org/10.1021/jp804715j.
[52] J. Baltrusaitis, V.H. Grassian, Carbonic acid formation from reaction of carbon dioxide and water coordinated to $Al(OH)_3$: a quantum chemical study, J. Phys. Chem. A 114 (6) (2010) 2350–2356, https://doi.org/10.1021/jp9097809.
[53] R.S. Alvim, I. Borges Jr., D.G. Costa, A.A. Leitao, Density-functional theory simulation of the dissociative chemisorption of water molecules on the MgO (001) surface, J. Phys. Chem. C 116 (1) (2012) 738–744, https://doi.org/10.1021/jp208007q.